PHYSICAL REVIEW D VOLUME 40, NUMBER 10 15 NOVEMBER 1989

Spherical inhomogeneous cosmologies and inflation: Numerical methods

Dalia S. Goldwirth* and Tsvi Piran†
Racah Institute for Physics, The Hebrew University, Jerusalem 91904, Israel
(Received 1 May 1989; revised manuscript received 29 June 1989)

We describe a spherically symmetric code for inhomogeneous cosmological problems. Our main goal is to study the onset of inflation under inhomogeneous conditions. We would like to explore the influence of inhomogeneity on inflation. In particular we address the question of whether large inhomogeneity during the very early Universe can prevent the Universe from entering an inflationary era. In this paper we describe the equations, the numerical techniques, tests, and some preliminary results. A detailed discussion of the results will follow in a subsequent paper.

I. INTRODUCTION

One of the main objectives for the introduction of the inflationary paradigm[1] was to explain the large-scale homogeneity of the Universe. Still most of the current work on inflation is done within the context of a homogeneous Robertson-Walker universe, or with small perturbations around it.[2,3] It is not clear whether an inhomogeneous universe (which needs an inflationary period to homogenize it) can actually enter into an inflationary phase. Our objective is to study the onset of inflation under inhomogeneous initial conditions. We would like to do this for a general three-dimensional (3D) case, but as a first step we consider 1D spherically symmetric cosmology. We focus on spherically symmetric cosmology since such perturbations resemble (topologically) realistic perturbations more than any other 1D model.

We have constructed a general-relativistic spherically symmetric code for solving inhomogeneous cosmological problems with a massive scalar field and a radiation field. The radiation is described by a massless scalar field coupled to the massive scalar field via a potential term. This radiation field enables us to explore the effects of thermal fluctuation on the evolution of the scalar field during the preinflationary period. An alternative way is to use a perfect fluid with $\Gamma=\frac{3}{4}$ and $n=0$. In the latter case the scalar field and the radiation field are coupled only gravitationally.

The code can simulate closed, flat, and open cosmologies. However, in this discussion we focus on closed comologies. The motivation comes from quantum-mechanical considerations that suggest that the Universe is closed.[4] Furthermore, the formation of the outer boundary conditions is clear in this case. We will describe the general case but when we have to be specific, like in the case of outer boundary conditions, we will refer to closed geometries.

The code differs in many aspects from spherically symmetric collapse codes.[5] The overall topology is closed and the space-time is not asymptotically flat. This changes drastically the outer boundary conditions. The cosmological expansion leads to a different natural slicing condition ($\mathrm{Tr}K=$const rather than $\mathrm{Tr}K=0$, and in fact even this is not always possible). Finally, the basic source terms are different. Collapse codes generally deal with perfect fluids and we consider scalar fields. The introduction of this new source changes some of the common features of the solutions. In particular one has to generalize the usual York procedure[6,7] for the initial-value problem.

In Sec. II we describe the field equations that follow to some extent the outline of Piran.[8] The initial-value problem is discussed in Sec. III. In Sec. IV we present the numerical methods that we have used. Finally, in Sec. V we exhibit several tests and some preliminary results.

We use the units $c=8\pi G=1$.

II. THE FIELD EQUATIONS

A. Geometry

We write the metric in a way convenient for cosmological problems. We use the generalized (we use the term generalized to denote the difference from the common spherical isotropic coordinate system which does not include the Friedmann factor $\sin^2\chi$, it reduces to the usual isotropic coordinates[9] when $\sin\chi=r$) spherical isotropic metric which for closed manifolds has the form

$$ds^2=-(N^2-R^2\beta^2)dt^2+2R^2\beta\,d\chi\,dt+R^2(d\chi^2+\sin^2\chi\,d\Omega^2)\,, \tag{2.1}$$

where $0\le\chi\le\pi$, and R, N, and β are functions of χ and t. When the cosmology is open we replace $\sin\chi$ by $\sinh\chi$ or by χ.

York[6] has suggested to use $\mathrm{Tr}K=$const slices for cosmological problems. Goddard has shown,[10] given one such slice, that such a foliation (of a closed cosmology) will exist if the strong energy condition is satisfied. This gauge has worked well in numerical cosmological studies[3] investigated so far. However, the energy-momentum tensor of the scalar field does not satisfy the strong energy condition during the inflationary epoch and it is not certain that such a foliation exists. We demonstrate this point numerically later. Hence, for closed cosmologies (dominated by a scalar field) we must choose another slicing condition. We are investigating now several slicing conditions that will have the same features as the $\mathrm{Tr}K=$const slices for closed manifolds. However, in this

paper we focus on the numerical scheme which was set for the general case; i.e., it is independent of the slicing conditions. We will discuss the issue of different slicing conditions in a separate publication. To obtain preliminary results for closed cosmologies we have used the gauge $\mathrm{Tr}K=\text{const}$ whenever it was possible. Otherwise we have used the gauge $N=1$ which, in spite of all its known[6,8,11] problems, was satisfactory. For flat and open cosmologies we have used $\mathrm{Tr}K=\text{const}$ slices.

The form of the spatial metric determines the shift vector equation. Using the metric form [Eq. (2.1)] we find two different evolution equations for the metric function $R(\chi,t)$: one from the equation for $\gamma_{\chi\chi,t}$,

$$\frac{\partial R}{\partial t}=-NR\tilde{K}-\tfrac{1}{3}NR\ \mathrm{Tr}K+\beta R_{,\chi}+R\beta_{,\chi}\ , \tag{2.2}$$

and the other from the equation for $\gamma_{\theta\theta,t}$,

$$\frac{\partial R}{\partial t}=\frac{N\tilde{K}}{2}R-\tfrac{1}{3}NR\ \mathrm{Tr}K+\beta R_{,\chi}+\beta R\cot\chi\ . \tag{2.3}$$

A tilde above a tensor denotes its traceless part. In particular $\tilde{K}_{ij}$ is the traceless part of the extrinsic curvature tensor:

$$\tilde{K}_{ij}=K_{ij}-\tfrac{1}{3}\gamma_{ij}\mathrm{Tr}K\ . \tag{2.4}$$

Because of the spherical symmetry $\tilde{K}\equiv\tilde{K}^{\chi}_{\chi}=-\frac{1}{2}\tilde{K}^{\theta}_{\theta}=-\frac{1}{2}\tilde{K}^{\phi}_{\phi}$. In order that Eqs. (2.2) and (2.3) will be consistent the shift vector β must satisfy

$$\sin\chi\left[\frac{\beta}{\sin\chi}\right]_{,\chi}=\tfrac{3}{2}N\tilde{K}\ . \tag{2.5}$$

Using Eq. (2.5) we rewrite the evolution equation for R in the form

$$\frac{\partial R}{\partial t}=-\tfrac{1}{3}NR\ \mathrm{Tr}K+\frac{1}{3}\frac{1}{R^2\sin^2\chi}(\beta R^3\sin^2\chi)_{,\chi}\ . \tag{2.6}$$

The evolution equation for $\tilde{K}$ is

$$\frac{\partial\tilde{K}}{\partial t}=-\tfrac{2}{3}N^{\chi}_{;\chi}+N(\tilde{\mathcal{R}}^{\chi}_{\chi}+\tilde{K}\ \mathrm{Tr}K-\tilde{S}^{\chi}_{\chi})+\beta\tilde{K}_{,\chi}\ , \tag{2.7}$$

where $\tilde{\mathcal{R}}^{\chi}_{\chi}$ is the traceless part of the Ricci tensor

$$\tilde{\mathcal{R}}^{\chi}_{\chi}=-\frac{2}{3}\left[\frac{R_{,\chi\chi}}{R^3}-\frac{2R^2_{,\chi}}{R^4}-\frac{R_{,\chi}\cos\chi}{R^3\sin\chi}\right] \tag{2.8}$$

and $\tilde{S}^{\chi}_{\chi}$ is the traceless part of S^{χ}_{χ} (S_{ij} is the spatial part of the energy-momentum tensor $T_{\mu\nu}$, i.e., $S_{ij}\equiv T_{ij}$).

The evolution equation for $\mathrm{Tr}K$ is

$$\frac{\partial\,\mathrm{Tr}K}{\partial t}=-N^{\chi}_{;\chi}+N[\tfrac{3}{2}\tilde{K}^2+\tfrac{1}{3}(\mathrm{Tr}K)^2+\tfrac{1}{2}(\mathrm{Tr}S+\bar{\rho})]+\beta\,\mathrm{Tr}K_{,\chi}\ , \tag{2.9}$$

where $\bar{\rho}\equiv N^2T^{00}$ and $\mathrm{Tr}S=S^j_j\equiv T^j_j$. For the gauge $\mathrm{Tr}K=\text{const}$ we chose an arbitrary function of the time $F(t)$ and impose the condition $\partial\,\mathrm{Tr}K/\partial t=F(t)$. This yields a linear elliptic equation for the lapse function N:

$$N^{\chi}_{;\chi}=\frac{1}{\sin^2\chi R^3}(R\sin^2\chi N_{,\chi})_{,\chi}=N[\tfrac{3}{2}\tilde{K}^2+\tfrac{1}{3}(\mathrm{Tr}K)^2+\tfrac{1}{2}(\mathrm{Tr}S+\bar{\rho})]+\beta\,\mathrm{Tr}K_{,\chi}-F(t)\ . \tag{2.10}$$

The Hamiltonian constraint is given by

$$\mathcal{R}=2\bar{\rho}+\tfrac{3}{2}\tilde{K}^2-\tfrac{2}{3}(\mathrm{Tr}K)^2\ , \tag{2.11}$$

where $\mathcal{R}$ is the Ricci scalar:

$$\mathcal{R}=-\frac{4}{R^3}\left[R_{,\chi\chi}+2\frac{R_{,\chi}\cos\chi}{\sin\chi}-\frac{R^2_{,\chi}}{R}\right]+\frac{6}{R^2}\ . \tag{2.12}$$

The momentum constraint has only one nontrivial equation:

$$\frac{\partial}{\partial\chi}(R^3\sin^3\chi\tilde{K})=R^3\sin^3\chi(J_{\chi}+\tfrac{2}{3}\mathrm{Tr}K_{,\chi})\ , \tag{2.13}$$

where

$$J_{\chi}\equiv NT^0_{\chi} \tag{2.14}$$

is the momentum flux.

These equations are supplemented by boundary conditions at the origin and at the outer radial boundary. The boundary condition at the origin are determined by regularity conditions:

$$\begin{aligned}&R=R_0(t)+O(\chi^2),\quad \tilde{K}+O(\chi^2)\ ,\\ &\mathrm{Tr}K=\mathrm{Tr}K_0(t)+O(\chi^2)\ ,\\ &N=N_0(t)+O(\chi^2),\quad \beta=O(\chi)\ .\end{aligned} \tag{2.15}$$

For closed cosmologies the outer boundary conditions (at $\chi=\pi$) are also determined from regularity considerations:

$$\begin{aligned}&R=R_{\pi}(t)=O((\pi-\chi)^2),\quad \tilde{K}=O((\pi-\chi)^2)\ ,\\ &\mathrm{Tr}K=\mathrm{Tr}K_{\pi}(t)+O((\pi-\chi)^2)\ ,\\ &N=N_{\pi}(t)+O((\pi-\chi)^2),\quad \beta=O(\pi-\chi)\ .\end{aligned} \tag{2.16}$$

For open cosmologies these boundary conditions are determined by asymptotic considerations which we will discuss elsewhere.

In closed cosmologies we can also impose a reflection symmetry around $\pi/2$. In this case it is adequate to solve the evolution of only half of the Universe with the following outer boundary conditions at $\pi/2$:

$$\begin{aligned}&R=R_{\pi/2}(t)+O((\pi/2-\chi)^2)\ ,\\ &\tilde{K}=\tilde{K}_{\pi/2}(t)+O((\pi/2-\chi)^2)\ ,\\ &\mathrm{Tr}K=\mathrm{Tr}K_{\pi/2}(t)+O((\pi/2-\chi)^2)\ ,\\ &N=N_{\pi/2}(t)+O((\pi/2-\chi)^2)\ ,\\ &\beta=O(\pi/2-\chi)\ .\end{aligned} \tag{2.17}$$

B. The scalar-field equations

We consider two types of scalar fields: a massive scalar field Φ, which acts as the source that drives inflation, and

a massless one Ψ, which plays the role of a radiation field (the "average pressure" of a massless scalar field is $\bar{p}=\rho/3$). The code can handle general potentials for the scalar field. We have focused our attention on two types of "chaotic inflation" potentials, $V=M^2\Phi^2/2$ and $V=\lambda\Phi^4/4$, and on a "new-inflation"-type potential, $V=\lambda(\Phi^2-\sigma^2)^2/4$. The scalar radiation field Ψ does not have a potential of its own but it can be coupled to the massive scalar field via a potential term of the form $g\Phi^2\Psi^2$ (g being the coupling constant).

The scalar field Φ evolves according to the Klein-Gordon equation

$$\Phi^{\mu}_{;\mu}\equiv\frac{1}{NR^3\sin^2\chi}\left[\frac{\partial}{\partial\chi}\left\{NR^3\sin^2\chi\left[\left[\frac{1}{R^2}-\frac{\beta^2}{N^2}\right]\Phi_{,\chi}+\frac{\beta}{N^2}\Phi_{,t}\right]\right\}+\frac{\partial}{\partial t}\left[NR^3\sin^2\chi\left[-\frac{1}{N^2}\Phi_{,t}+\frac{\beta}{N^2}\Phi_{,\chi}\right]\right]\right]=\frac{dV}{d\Phi}\ . \tag{2.18}$$

We define the conjugate momentum

$$\Pi\equiv\frac{R^3}{N}(\beta\Phi_{,\chi}-\Phi_{,t}) \tag{2.19}$$

and replace Eq. (2.18) by two first-order partial differential equations:

$$\Phi_{,t}=\beta\Phi_{,\chi}-\frac{N}{R^3}\Pi \tag{2.20a}$$

and

$$\Pi_{,t}=\frac{1}{\sin^2\chi}\frac{\partial}{\partial\chi}(-NR\,\Phi_{,\chi}\sin^2\chi+\beta\Pi\sin^2\chi)+NR^3\frac{dV}{d\Phi}\ . \tag{2.20b}$$

The field Ψ evolves according to similar equations but its potential does not include a mass term.

The energy-momentum tensor of the scalar field has the form

$$T_{\mu\nu}=\Phi_{,\mu}\Phi_{,\nu}-\tfrac{1}{2}g_{\mu\nu}[g^{\alpha\beta}\Phi_{,\alpha}\Phi_{,\beta}+2V(\Phi)]\ . \tag{2.21}$$

The scalar-field sources (denoted by Φ in the subscript) in the gravitational equations are

$$\begin{aligned}
&\bar{\rho}_{\Phi}=\frac{1}{2}\left[\frac{\Phi^2_{,\chi}}{R^2}+\frac{\Pi^2}{R^6}+2V(\Phi)\right]\ ,\\
&\tilde{S}^{\chi}_{\chi\Phi}=\frac{2}{3}\frac{\Phi^2_{,\chi}}{R^2}\ ,\\
&\mathrm{Tr}S_{\Phi}=-\frac{\Phi^2_{,\chi}}{2R^2}+\frac{3}{2}\frac{\Pi^2}{R^6}-3V(\Phi)\ ,\\
&J_{\chi\Phi}=\frac{\Phi_{,\chi}\Pi}{R^3}\ .
\end{aligned} \tag{2.22}$$

Similar terms appear for Ψ with the obvious replacements. Note that $\bar{\rho}_{\Phi}$ and $J_{\chi\Phi}$ are independent of the lapse function N when they are expressed in terms of Π. This is an essential step whenever the sources are fields. It enables one to solve the initial-value problem (see Sec. III) in a gauge-independent way.

As for the geometry, regularity considerations determine the boundary conditions at both $\chi=0$ and $\chi=\pi$ for closed geometries (at $\chi=0$ for open geometries):

$$\begin{aligned}
&\Phi=\Phi_0(t)+O(\chi^2)\ ,\\
&\Pi=\Pi_0(t)+O(\chi^2)\ ,
\end{aligned} \tag{2.23}$$

and

$$\begin{aligned}
&\Phi=\Phi_{\pi}(t)+O((\pi-\chi)^2)\ ,\\
&\Pi=\Pi_{\pi}(t)+O((\pi-\chi)^2)\ .
\end{aligned} \tag{2.24}$$

When we impose reflection symmetry relative to $\chi=\pi/2$, the outer boundary conditions at $\pi/2$ are

$$\begin{aligned}
&\Phi=\Phi_{\pi/2}(t)+O((\pi/2-\chi)^2)\ ,\\
&\Pi=\Pi_{\pi/2}(t)+O((\pi/2-\chi)^2)\ .
\end{aligned} \tag{2.25}$$

Clearly, similar conditions hold for Ψ.

III. THE INITIAL-VALUE PROBLEM AND THE GENERALIZED YORK PROCEDURE

The initial data on a three-dimensional spatial hypersurface must satisfy the constraint equations. To obtain such data we use the general York[7] procedure. In the common York procedure one chooses a conformal metric γ_{ij} and initial guesses for TrK and $\tilde{K}$ and for the matter sources $\bar{\rho}$ and J_i, and solves the Hamiltonian constraint for a conformal factor ψ to obtain $g_{ij}=\psi^2\gamma_{ij}$. In this procedure it is essential to rescale $\tilde{K}$ and $\bar{\rho}$:

$$\hat{K}=\psi^{10}\tilde{K} \tag{3.1}$$

and

$$\hat{\rho}=\psi^8\bar{\rho}\ .$$

Because of the scaling the final matter sources are not the ones that we have selected initially. The Hamiltonian constraint becomes a nonlinear elliptic equation for the conformal factor ψ:

$$-8\Delta_{\gamma}\psi+\mathcal{R}(\gamma)\psi^{-1}=-\tfrac{2}{3}(\mathrm{Tr}K)^2\psi^5+\tfrac{3}{2}\hat{K}^2\psi^{-7}+2\hat{\rho}\psi^{-3}\ . \tag{3.2}$$

In the generalized spherical iosotropic coordinates, γ_{ij} is specified by a scale factor R^* and $\mathcal{R}(\gamma)$ is given by Eq. (2.12) for R^*. We choose an initial distribution Φ_i for the scalar field and we obtain $\bar{\rho}_{\Phi}$ using Eq. (2.22). Since we need the scalar field Φ rather than $\bar{\rho}$ we have to specify a scaling law for Φ rather than for $\bar{\rho}$. Direct scaling of field variables has been done before, but in the present case new terms arise in the equation for ψ. This scaling law depends on the potential [see Eq. (2.22)]. For a single massive scalar field we choose

$$\hat{\Phi}=\psi^3\Phi \tag{3.3}$$

This rescaling results in a new gradient term in Eq. (2.22),

$$\frac{\Phi_{,\chi}}{R}=\frac{1}{R^*}(-3\psi^{-6}\hat{\Phi}\psi_{,\chi}+\psi^{-5}\hat{\Phi}_{,\chi}) , \tag{3.4}$$

and the Hamiltonian constraint becomes

$$\begin{aligned}-8\Delta_\gamma\psi+\mathcal{R}(\gamma)\psi^{-1}=&-\tfrac{2}{3}(\mathrm{Tr}K)^2\psi^5+\tfrac{3}{2}\hat{K}^2\psi^{-7}\\&+2V(\psi^{-3}\Phi,\Psi)\psi^5\\&+\frac{1}{R^*}[9\hat{\Phi}^2\psi_{,\chi}^2\psi^{-7}-3(\hat{\Phi}^2)_{,\chi}\psi_{,\chi}\psi^{-6}\\&+\hat{\Phi}_{,\chi}^2\psi^{-5}] .\end{aligned} \tag{3.5}$$

For simplicity we choose $\tilde{K}=0$ and $\Pi=0$ so that the momentum constraint is satisfied automatically. With the initial γ_{ij} and $\hat{\Phi}$ we solve Eq. (3.5) for ψ and we obtain the "true" scale factor $R=\psi^2R^*$ which appears in g_{ij}. We rescale the scalar field according to Eq. (3.3): $\Phi_{\mathrm{new}}=\psi^{-3}\hat{\Phi}$. Like with any other York procedure algorithm, we end up with a matter distribution which is different from our initial guess.

An alternative, simpler approach to the initial-value problem is to add a radiation field (i.e., a massless scalar field) so that $\bar{\rho}$ is initially constant. The Hamiltonian constraint becomes a simple algebraic equation for R, which is constant on the initial slice. The easiest way to add the radiation field is to choose $\Pi_\Psi\neq0$ and $\Psi=0$. With this choice the current $\Psi_{,\chi}\Pi_\Psi$ vanishes and the momentum constraint is satisfied trivially with $\tilde{K}=0$ [see Eq. (2.13)]. In the cases that we present later the added radiation field decays rapidly and its addition does not change the nature of the results.

IV. NUMERICAL METHODS

A. The grid structure

We solve the equations by finite differencing on a staggered numerical grid maintaining second-order accuracy both in space and in time. We define two staggered spatial grid systems $\chi_a(j)$ and $\chi_c(j)$ where $j=1,\ldots,n$, with

$$\chi_a(1)=0,\quad \chi_a(j)=\chi_a(j-1)+d\chi_j \tag{4.1}$$

and

$$\chi_c(j)=\tfrac{1}{2}[\chi_a(j+1)+\chi_a(j)] .$$

For closed manifolds $\chi_a(n+1)=\pi$ [in the symmetric case $\chi_a(n+1)=\pi/2$]. All the variables are defined on the grid points χ_c except for the "velocitylike" variable β which is defined on χ_a. The grid points are not necessarily equally spaced. In particular we increase the density of grid points in places where we expect large gradients. In these cases we restrict the variation of $d\chi$ so that it will not vary by more then a few percent between neighboring grid points.

We add "false" grid points:

$$\begin{aligned}&\chi_c(0)=-\chi_c(1) ,\\&\chi_c(n+1)=2\chi_c(n)-\chi_c(n-1) .\end{aligned} \tag{4.2}$$

The definition of "false" values on these grid points enables us to satisfy the boundary conditions automatically, and allows us to treat all the "real" grid points on the same footing as internal grid points.

For the variables whose gradients vanish on the boundaries [see Eqs. (2.15)–(2.17) and (2.23)–(2.25)] we set the "false" boundary condition: $f_0=f_1$ and $f_{n+1}=f_n$. The equations for the variables that vanish on the boundaries are devised so that they satisfy this condition.

The variables are also staggered in time. Most of the variables are calculated at $0,\Delta t_1,\Delta t_1+\Delta t_2,\ldots$, except for $\tilde{K}$, $\mathrm{Tr}K$, β, and Π which are calculated at $\frac{1}{2}\Delta t_1$, $\Delta t_1+\frac{1}{2}\Delta t_2,\ldots$.

The time step is determined by the Courant condition which is represented here by the requirement that the interval $(dt,d\chi)$ is spacelike:

$$dt<\frac{R\,d\chi}{N+|\beta|R} . \tag{4.3a}$$

The Courant condition is sufficient for stability but not for accuracy. When terms such as $N\,\mathrm{Tr}KR$ or $dV/d\Phi$ dominate the right-hand side (RHS) of the evolution equations we must impose the additional requirement that R and Φ do not change too much in one time step, i.e., $\dot{R}\,dt/R<\epsilon$ and $\dot{\Phi}\,dt/\Phi<\epsilon$. These conditions yield

$$dt<\min\left[\frac{R\epsilon}{\dot{R}},\frac{\Phi\epsilon}{\dot{\Phi}}\right] . \tag{4.3b}$$

B. The numerics of the initial-value problem

We solve Eq. (3.5), which is a nonlinear elliptic equation, using a relaxation method. We finite difference Eq. (3.5) as

$$A_p\psi_{j+1}+B_p\psi_{j-1}+C_p\psi_j+E_p=\mathrm{Resid}(\psi) , \tag{4.4}$$

where

$$\begin{aligned}A_p&=-\frac{8}{\chi_{aj+1}-\chi_{aj}}\frac{1}{\sin^2\chi_{cj}R_j^{*3}}\left[\frac{\sin^2\chi_{aj+1}}{\chi_{cj+1}-\chi_{cj}}\frac{R_j^*+R_{j+1}^*}{2}\right] ,\\B_p&=-\frac{8}{\chi_{aj+1}-\chi_{aj}}\frac{1}{\sin^2\chi_{cj}R_j^{*3}}\left[\frac{\sin^2\chi_{aj}}{\chi_{cj}-\chi_{cj-1}}\frac{R_j^*+R_{j-1}^*}{2}\right] ,\\C_p&=-(A_p+B_p) ,\\E_p&=\tfrac{3}{2}\hat{K}^2\psi_j^{-7}-\tfrac{2}{3}(\mathrm{Tr}K)^2\psi_j^5+\mathcal{R}(\gamma)\psi_j^{-1}-2V(\psi_j^{-3}\Phi_j,\Psi_j)\psi^{-5}\\&\quad+\frac{1}{R_j^{*2}}\left[-9\hat{\Phi}_j^2\left[\frac{\psi_{j+1}-\psi_{j-1}}{\chi_{cj+1}-\chi_{cj-1}}\right]^2\psi_j^{-7}+6\hat{\Phi}_j\hat{\Phi}_{,\chi j}\left[\frac{\psi_{j+1}-\psi_{j-1}}{\chi_{cj+1}-\chi_{cj-1}}\right]^2\psi_j^{-6}-\hat{\Phi}_{,\chi j}^2\psi_j^{-5}\right] .\end{aligned} \tag{4.5}$$

We guess an initial ψ (usually $\psi_j=1$, for $j=1,\ldots,n$) and we iterate over Eq. (4.4) changing ψ_j to $\psi_j+\Delta\psi_j$ so that

$$\begin{aligned}\mathrm{Resid}(\psi_j+\Delta\psi)&\equiv\mathrm{Resid}(\psi_j)+\frac{\partial\,\mathrm{Resid}(\psi_j)}{\partial\psi_j}\Delta\psi_j=0\\&=\mathrm{Resid}(\psi_j)+\left[C_p+\frac{\partial E_p}{\partial\psi_j}\right]\Delta\psi_j\equiv\mathrm{Resid}(\psi_j)+e\,\Delta\psi_j=0\ ,\end{aligned}\tag{4.6}$$

i.e.,

$$\psi_{j\mathrm{new}}=\psi_j-\frac{\mathrm{Resid}(\psi_j)}{e}\omega\ .\tag{4.7}$$

ω is an over-relaxation parameter ($1<\omega<2$). After finding ψ_j (to the required accuracy) we replace R_j by $\psi_j^2R_j$, Φ_j by $\Phi_{j\mathrm{new}}=\psi_j^{-3}\hat{\Phi}_j$ (and $\tilde{K}_j$ by $\psi_j^{-10}\tilde{K}_j$).

C. The geometry evolution equation

The geometry evolution equations are Eqs. (2.6), (2.7), and (2.9). We solve the convective term $(\beta R^3\sin^2\chi)_{,\chi}$, of Eq. (2.6) using weighted first- and second-order-conserving flux terms.[9] The first-order flux is

$$F_1=\beta_j\sin^2\chi_{aj}\times\begin{cases}R_j^3, & \beta_j>0,\\ R_{j-1}^3, & \beta_j<0,\end{cases}\tag{4.8}$$

while the second-order flux is

$$F_2=\beta_j\sin^2\chi_{aj}\left[R_j^3\left[\frac{1}{2}+\frac{\beta_j\Delta t}{d\chi}\right]+R_{j-1}^3\left[\frac{1}{2}-\frac{\beta_j\Delta t}{d\chi}\right]\right]\ .\tag{4.9}$$

F_2 interpolates R^3 to a distance $\beta\Delta t$ backwards from the zone boundary at χ_{aj}. This is the value of R^2 which would be carried by β to the zone boundary in one time step. If the gradients are large we use the first-order flux term F_1 while if the gradients are small we use the second-order flux terms F_2. The weighing factor W between the two terms is

$$W=\min\left\{\frac{R_j^3-R_{j-1}^3}{R_{j-1}^3},1\right\}\tag{4.10}$$

and the weighted flux at (χ_{aj}) is

$$F_j=WF_1+(1-W)F_2\ .\tag{4.11}$$

The new value of R_j due to the flux term is

$$R_j=R_j+\Delta t\frac{\cos\chi_{cj}}{R_j^2}\frac{F_{j+1}-F_j}{\sin^3\chi_{aj+1}-\sin^3\chi_{aj}}\ .\tag{4.12}$$

After calculating the contribution of the flux term we add the contribution of the second term in Eq. (2.6):

$$R_j=\frac{1-\frac{\Delta t}{6}N_j\mathrm{Tr}K_j}{1+\frac{\Delta t}{6}N_j\mathrm{Tr}K_j}R_j\ .\tag{4.13}$$

The flux terms $\beta f_{,\chi}$ in Eqs. (2.7) and (2.9) (where f stands for $\tilde{K}$ or for $\mathrm{Tr}K$) are also evaluated using a flux-conserving method, but in this case

$$\begin{aligned}F_1&=\begin{cases}\bar{\beta}F_j, & \bar{\beta}<0\ ,\\ \bar{\beta}F_{j+1}, & \bar{\beta}>0\ ,\end{cases}\\F_j&=\frac{f_j-f_{j-1}}{\chi_{cj}-\chi_{cj-1}}\ ,\\F_{j+1}&=\frac{f_{j+1}-f_j}{\chi_{cj+1}-\chi_{cj}},\quad\bar{\beta}=\frac{\beta_{j+1}+\beta_j}{2}\ ,\end{aligned}\tag{4.14}$$

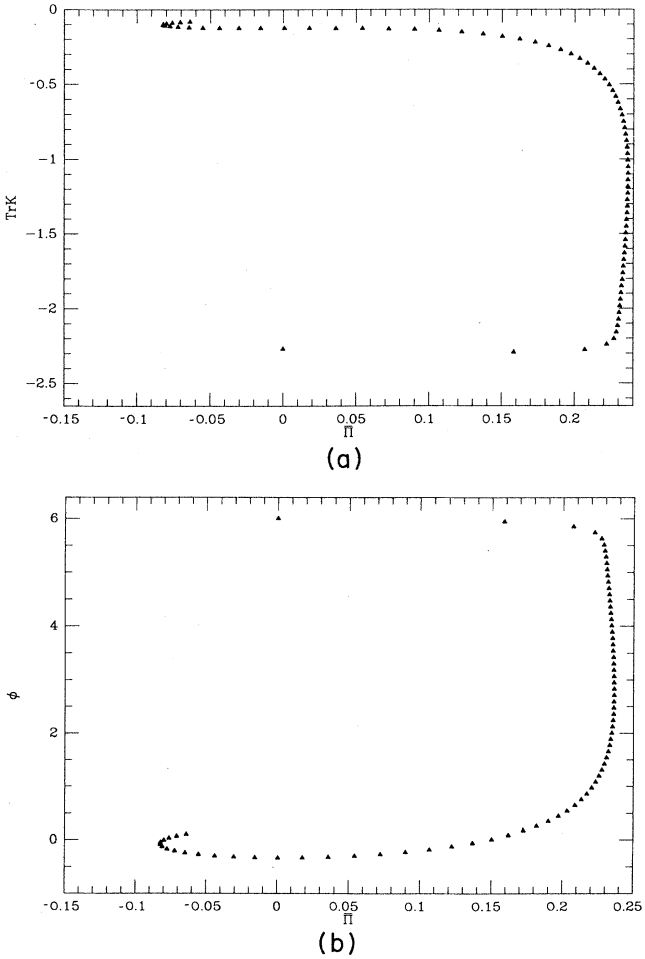

FIG. 1. Homogeneous solution with a massive scalar field. The initial conditions are $R=6$, $\mathrm{Tr}K=-2.35$, $\Phi=6$, and $\Pi=0$. Note that the $\bar{\Pi}\approx$const phase represents an inflationary period. The oscillations in $\bar{\Pi}$ and Φ describe regular evolution after inflation. (a) $\mathrm{Tr}K$ vs $\bar{\Pi}$; the temporal evolution is in an increasing $\mathrm{Tr}K$ direction. (b) Φ vs $\bar{\Pi}$; the temporal evolution is in a decreasing Φ direction.

and

$$F_2=\frac{1}{\chi_{aj+1}-\chi_{aj}}\{\beta_{j+1}F_{j+1}[(\chi_{aj+1}-\chi_{cj})+\bar{\beta}\Delta t] +\beta_j F_j[(\chi_{cj}-\chi_{aj})-\bar{\beta}\Delta t]\} . \quad (4.15)$$

F_2 is the interpolation of $\beta f_{,\chi}$, which is calculated at χ_{aj} and χ_{aj+1}, to the point $\chi_{cj}+\bar{\beta}\Delta t$. The weighted flux is

$$\beta f_{,\chi}=WF_1+(1-W)F_2 . \quad (4.16)$$

The other terms in Eqs. (2.7) and (2.9) are solved using

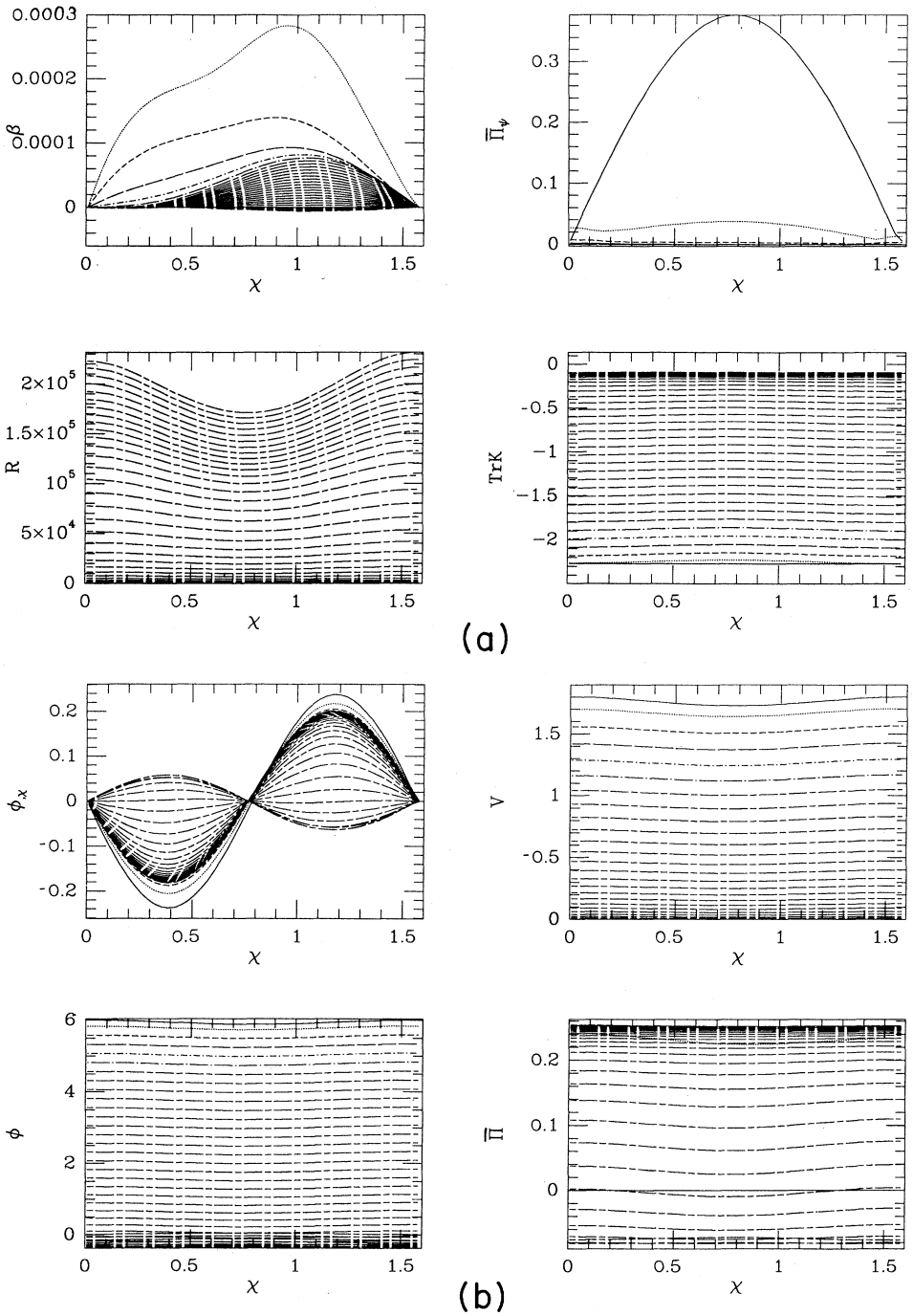

FIG. 2. Perturbations around a homogeneous solution, for $A=0.01$ with $N=1$. The solid lines describe the initial conditions and the other lines represent the evolution in time. The following time slices are described by the dotted lines, the short-dashed lines, the long-dashed lines, dashed-dotted lines, long-dashed-dotted lines, etc. This time sequence is best manifested in the graph of TrK vs χ where the time increases with TrK. (a) R, TrK, β, and $\bar{\Pi}_\Psi$ vs χ. (b) Φ, $\Phi_{,\chi}$, $\bar{\Pi}$, and V vs χ on different time slices.

standard finite-difference methods preserving second-order accuracy.

When we use $\mathrm{Tr}K=\text{const}$ slices we solve Eq. (2.10) for the lapse. This is a linear elliptic equation with boundary conditions given on both sides. Like Eq. (3.5), we solve it using an over-relaxation method.

We integrate Eq. (2.5) for β_{j-1} $(j=n-1,n-2,\ldots,2)$ starting from $\chi=\pi/2$, where $\beta=\beta_n=0$:

$$\beta_{j-1}=-\tfrac{3}{2}(\chi_{aj}-\chi_{aj-1})N_j\tilde{K}_j\frac{\sin\chi_{aj-1}}{\sin\chi_{cj}}+\beta_j\frac{\sin\chi_{aj-1}}{\sin\chi_{cj}}\ . \tag{4.17}$$

At $\chi=0$ Eq. (2.5) ensures that $\beta(0)=0$.

We finite difference the momentum constraint and solve it for $\tilde{K}_{j+1}$:

$$\tilde{K}_{j+1}=\frac{1}{R^3_{j+1}\sin^3\chi_{cj+1}}\{\tilde{K}_jR^3_j\sin^3\chi_{cj}+\sin^3\chi_{aj+1}[(\Phi_{j+1}-\Phi_j)\Pi_{j+1/2}+\tfrac{2}{3}R^3_{j+1/2}(\mathrm{Tr}K_{j+1}-\mathrm{Tr}K_j)]\}\ . \tag{4.18}$$

We begin by calculating $\tilde{K}$ at χ_{a2} using the boundary condition $\tilde{K}(\chi=0)=0$. $\tilde{K}$ is specified on middle points grid, i.e, χ_c so we interpolate $\tilde{K}(\chi_{a2})$ to find $\tilde{K}_1$ which is specified at χ_{c1} $[\tilde{K}(\chi_{c1})=\tilde{K}(\chi_{a2})/4]$.

D. Scalar fields

The scalar-field evolution is determined by Eqs. (2.20a) and (2.20b) for $\dot{\Phi}$ and $\dot{\Pi}$. The evolution equation for Π [Eq. (2.20b)] contains a convective term of the form $(\sin^2\chi\beta\Pi)_{,\chi}$ which we solve using the same flux-conserving method used for the metric function R (see Sec. IV C). The term $\beta\Phi_{,\chi}$ which appears in the evolution equation for Φ [Eq. (2.20a)] is evaluated like the term $\beta\tilde{K}_{,\chi}$ (see Sec. IV C). The numerical methods for the solution of Eq. (2.20b) do not depend on the form of the potential and the code can work with potentials corresponding to chaotic inflation (such as $m\Phi^2/2$ or $\lambda\Phi^4/4$) and with potentials corresponding to "new inflation" [such as $\lambda(\Phi^2-\sigma^2)^2/4$].

E. The overall scheme

We solve, first, the initial-value problem. Once we have proper initial data we proceed with the following evolution loop. The order in which we evolve the variables is determined by their time staggering and the way they appear in the equations.

Start.

(1) Evaluate the time step.

(2) Calculate the shift vector β [Eq. (2.5)].

(3) Evolve $\mathrm{Tr}K$ [Eq. (2.9)] or determine it from $F(t)$.

(4) Solve extrinsic curvature $\tilde{K}$ from the momentum constraint [Eq. (2.13)].

(5) Evolve the momentum of the massive scalar field Π_Φ [Eq. (2.20b)].

(6) Evolve the momentum of the massless scalar field Π_Ψ [Eq. (2.20b) for Π_Ψ].

(7) Evolve the metric function R [Eq. (2.6)].

(8) Evolve the massive scalar field Φ [Eq. (2.20a)].

(9) Evolve the massless scalar field (the radiation field) Ψ [Eq. (2.20a) for Ψ].

(10) If we work in the gauge $\mathrm{Tr}K=\text{const}$, determine

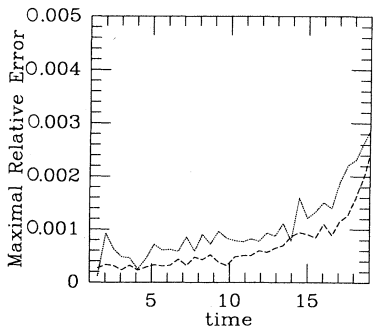

FIG. 4. Maximal relative errors in Φ (dashed line) and in R (dotted line) between runs with 200 and 300 grid points, for initial data with $R=6$, $\mathrm{Tr}K=-2.43$, and $\Delta^2=0.8$.

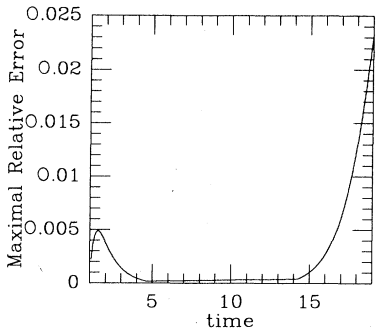

FIG. 3. The relative error in the Hamiltonian constraint for evolution of a narrow Gaussian Φ distribution ($\Delta^2=0.8$) (see Fig. 6 for the details of the evolution).

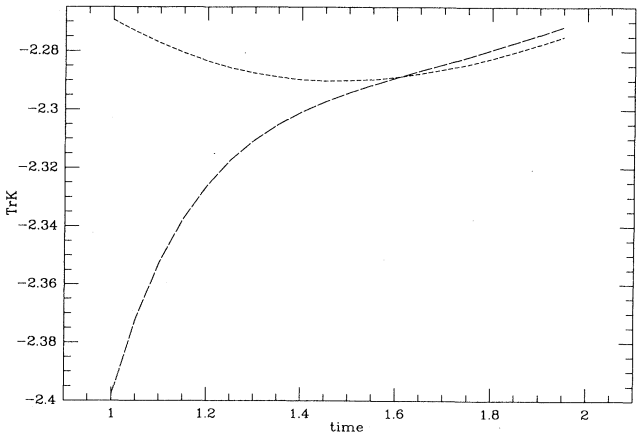

FIG. 5. $\mathrm{Tr}K$ vs t, for homogeneous evolution with just scalar field (short-dashed line) and with both scalar field and radiation (long-dashed line).

the lapse N [Eq. (2.10].

Return to start.

V. TESTS AND PRELIMINARY RESULTS

All the results presented in this section are with closed topology. When we discuss "chaotic inflation" the scalar field is massive, with $M=\sqrt{0.1}$. When we discuss "new inflation" the potential V equals $\lambda(\Phi^2-\sigma^2)^2/4$, with $\lambda=0.01$ and $\sigma=4$. The coupling term between the radiation field and the scalar field is set to zero in the following calculations.

We have used, first, homogeneous initial conditions. With this initial data the evolution remains, as it should, homogeneous. Homogeneity is maintained to the numerical accuracy of the calculations, i.e., to within ten significant digits or better. The results of a homogeneous run are best presented by the trajectory of the solution in

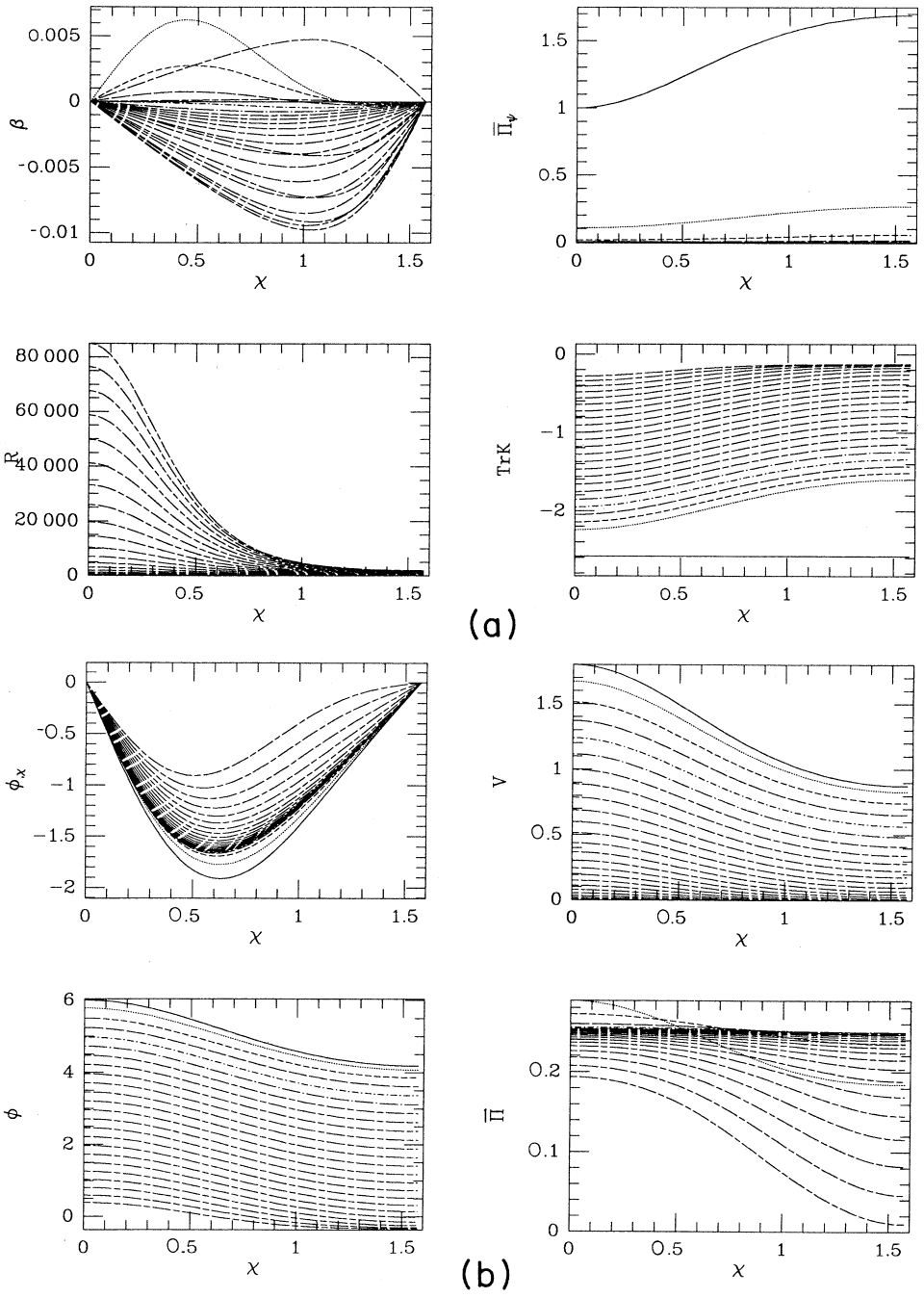

FIG. 6. Evolution of a universe with an isocurvature initial data combined of a massive scalar field with $\Delta^2=0.8$ and a radiation field. $N=1$ slicing condition (for details about the direction of the time see Fig. 2). (a) R, TrK, β, and $\bar{\Pi}_\Psi$ vs χ. (b) Φ, $\Phi_{,\chi}$, $\bar{\Pi}$, and V vs χ on different time slices.

the $(\overline{\Pi}, \mathrm{Tr}K)$ plane and in the $(\overline{\Pi}, \Phi)$ plane, where $\overline{\Pi} \equiv \Pi / R^3$. Belinski, Grishchuk, Khalatnikov, and Zel'dovich and Piran and Williams[12] have pointed out that during inflation the second-derivative term in the Φ equation is negligible and therefore $\overline{\Pi}$ is approximately a constant. This is clearly seen in Fig. 1.

In order to check whether perturbations grow due to numerical instability we have added to the homogeneous initial data small initial perturbations, of the form

$$\delta\Phi = A \cos 4\chi \ , \tag{5.1}$$

for several values of A $(0.001 < A < 0.1)$. These pertur-

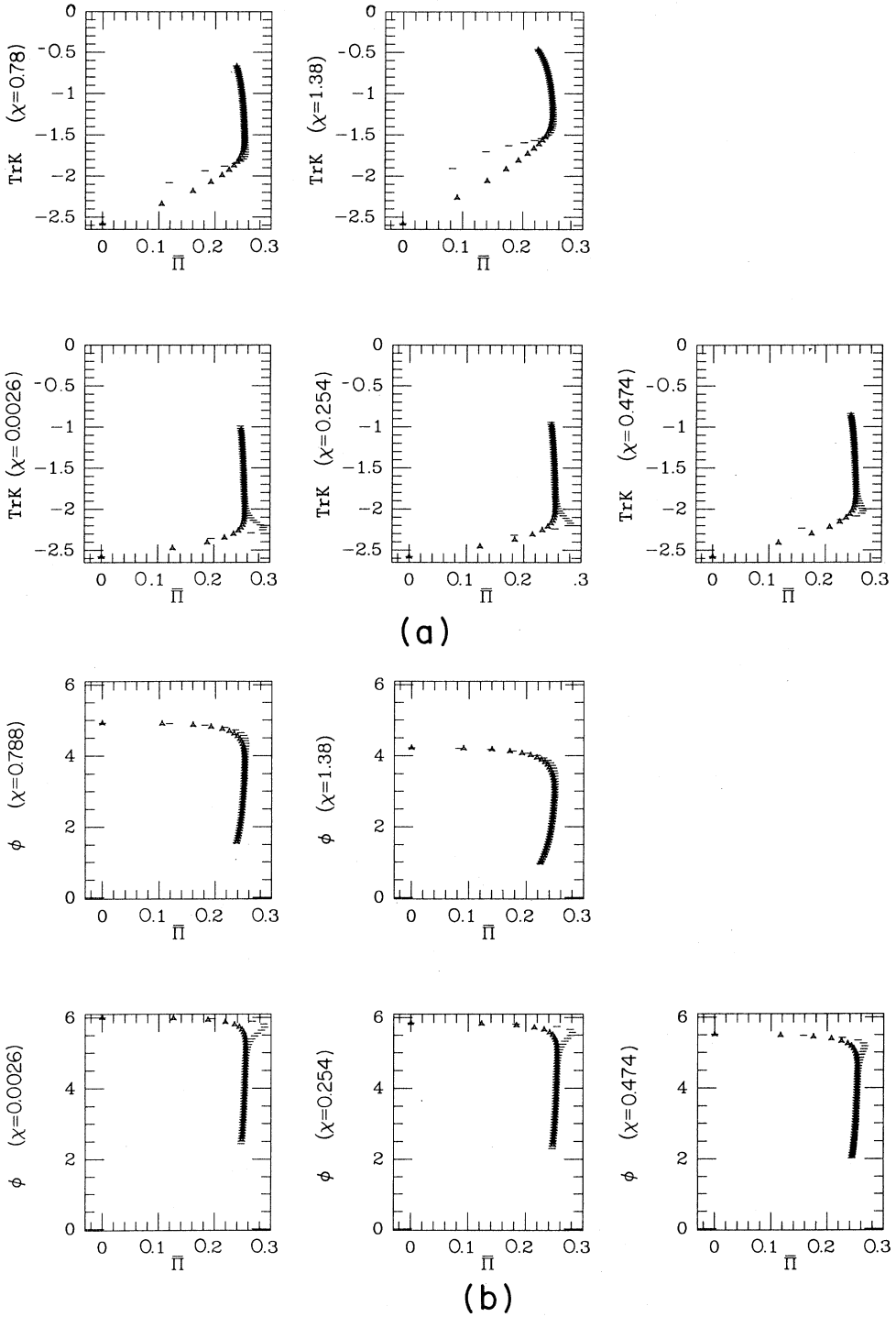

FIG. 7. (a) TrK vs $\overline{\Pi}$ trajectories of several points in an inhomogeneous solution (bars) of Fig. 6 and the same curves in a homogeneous solution with the same initial data (triangles). The temporal evolution is in an increasing TrK direction. (b) Trajectories in the $\overline{\Pi}$, Φ plane for the same points. The temporal evolution is in a decreasing Φ direction.

bations do not grow during the inflationary period but, as the horizon increases rapidly, they become spread just as expected from perturbations on a de Sitter universe.[13] Results of such an evolution are shown in Fig. 2.

Another test for the accuracy of the code is provided, in general-relativistic calculations, by the degree in which the Hamiltonian constraint is satisfied. In the perturbation calculations which are almost homogeneous, the relative error in the Hamiltonian constraint is less then 10^{-3}. Clearly, this accuracy is reduced when we introduce larger inhomogeneity. Still, even when the initial Φ was a narrow Gaussian [where Δ^2, the width of the Φ distribution was 0.05, see Eq. (5.3), the relative error in the Hamiltonian constraint was below 10^{-1}]. Figure 3 de-

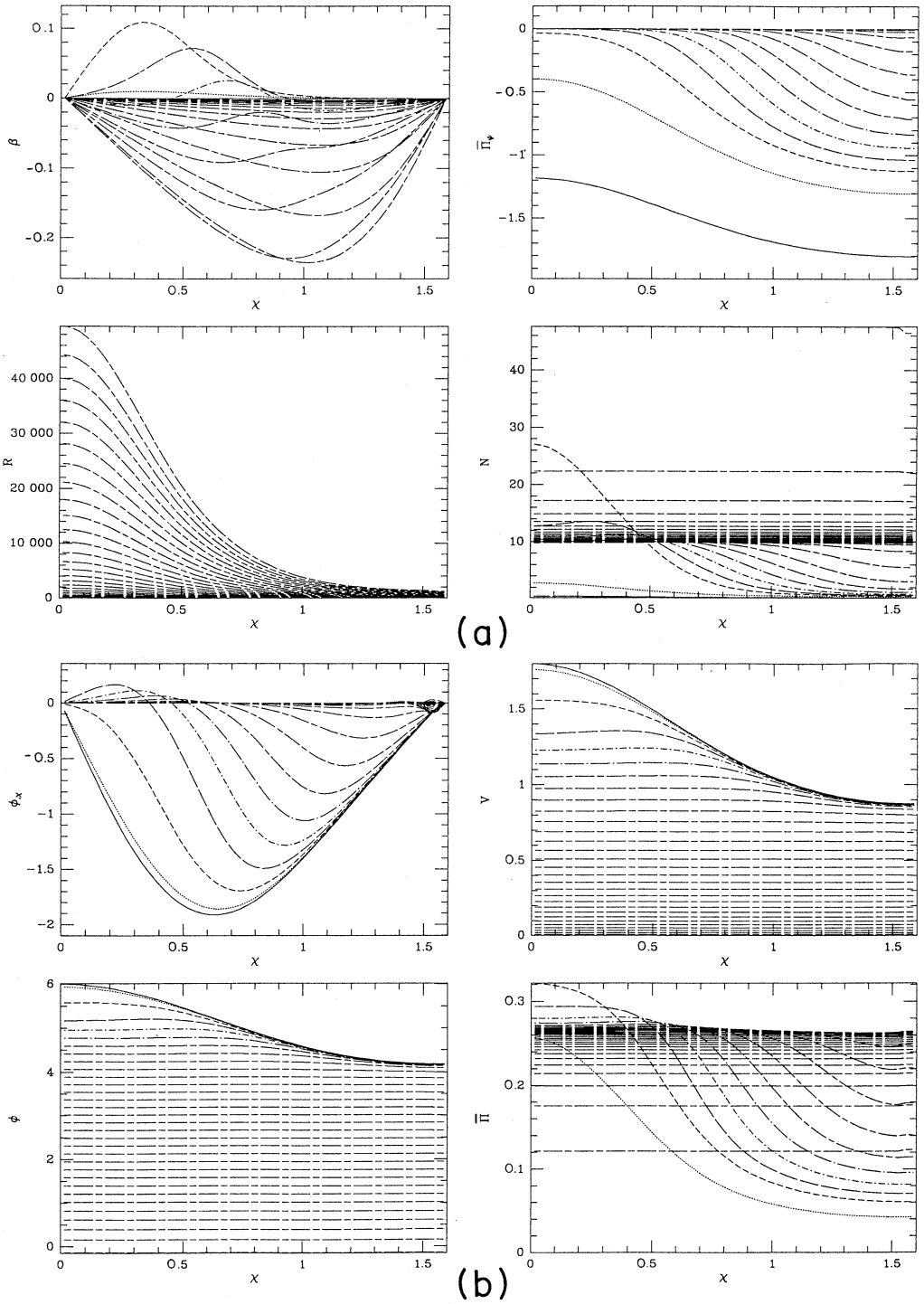

FIG. 8. Evolution of a universe with the same initial data as in Fig. 6 but with $\mathrm{Tr}K=$const slicing condition: (a) R, N, β, and $\bar{\Pi}_\Psi$ vs χ. (b) Φ, $\Phi_{,\chi}$, $\bar{\Pi}$, and V vs χ on different time slices.

scribes the variation of the error in the Hamiltonian constraint with time along evolution with ($\Delta^2=0.8$).

The final test, that we present here, is the usual numerical test of comparisons of the results with different grid sizes. We compare, in Fig. 4, the evolution of the same initial data with 200 and 300 grid points. The error grows during the evolution but even with relatively small number of grid points it remains below 0.5%.

When the Universe contains only a massive scalar field the strong energy condition[14] is violated when the inflationary phase begins. For a closed cosmology this results in a breakdown of the TrK=const slicing condition. To see this, we consider, first a homogeneous solution. Substitution of TrK from Eq. (2.11) and $\bar{\rho}$ from Eq.

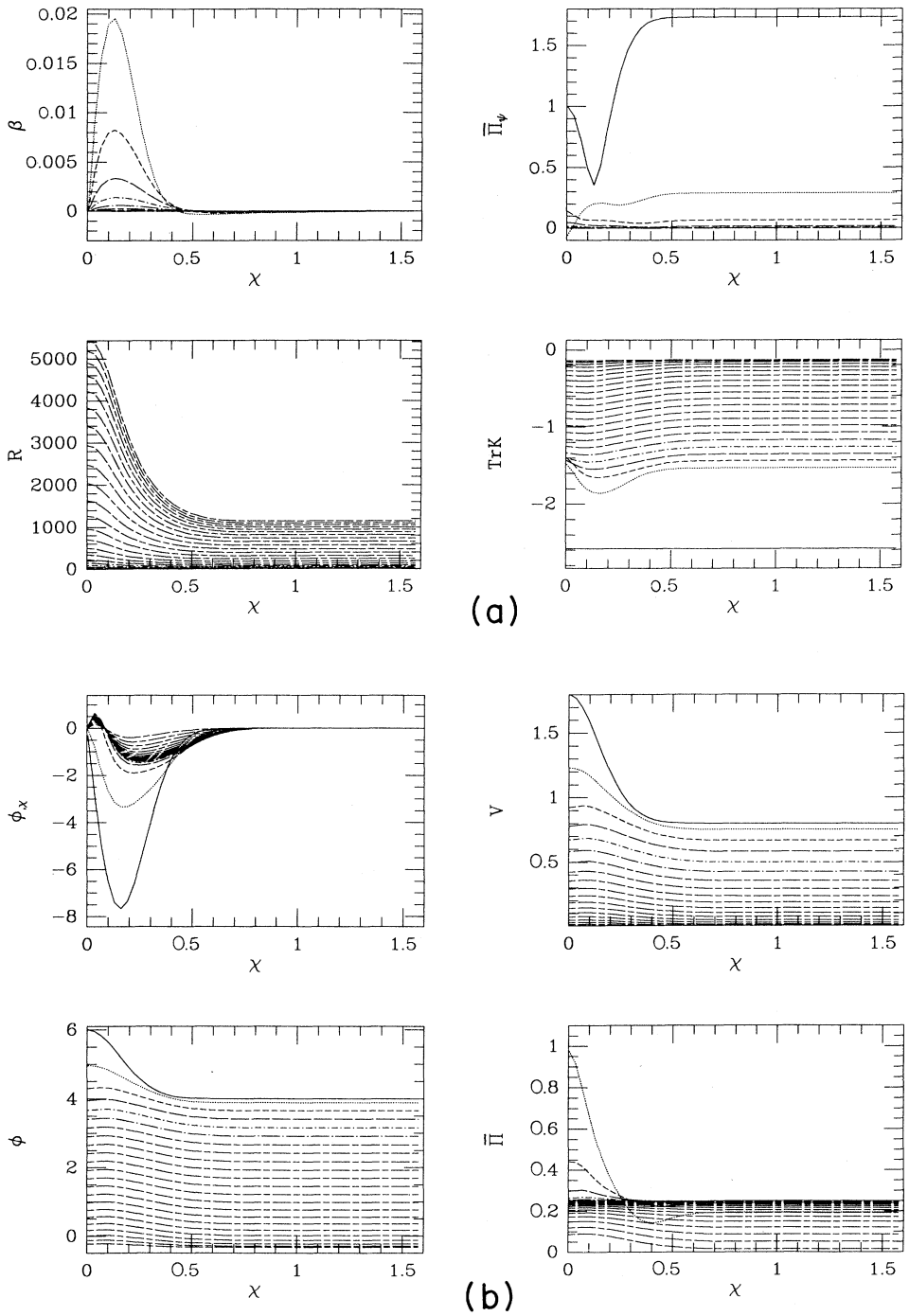

FIG. 9. Evolution of a universe with an isocurvature initial data constructed from a massive scalar field with $\Delta^2=0.05$ and a radiation field. $N=1$ slicing condition (for details about the direction of the time see Fig. 2). (a) R, TrK,β, and $\bar{\Pi}_\psi$ vs χ. (b) Φ, $\Phi_{,\chi}$, $\bar{\Pi}$, and V vs χ on different time slices.

(2.22) in Eq. (2.10) yields

$$N\left[\frac{3}{2}\frac{\Pi^2}{R^6}-\frac{3}{R^2}\right]=\frac{\partial \mathrm{Tr}k}{\partial t}\equiv F(t)\ . \tag{5.2}$$

$\partial \mathrm{Tr}k/\partial t$ is negative and TrK *decreases* if $3\Pi^2/2R^3 < 3/R^2$. In Fig. 5 we show TrK for two homogeneous solutions. The dip in TrK is evident in one of the solutions. In this case TrK = const slicing exists, but TrK is not a monotonic function of time. Clearly, one cannot use in this case Eq. (2.10) with a positive $F(t)$. When we add a radiation field, the combined energy-momentum tensor can satisfy the energy condition and monotonic TrK = const slicing might exist (see Fig. 5). The same phenomenon occurs with inhomogeneous data. When we try to use TrK = const with just a scalar field the slicing condition breaks down when inflation begins. The nature of this breakdown is similar to the problem with homo-

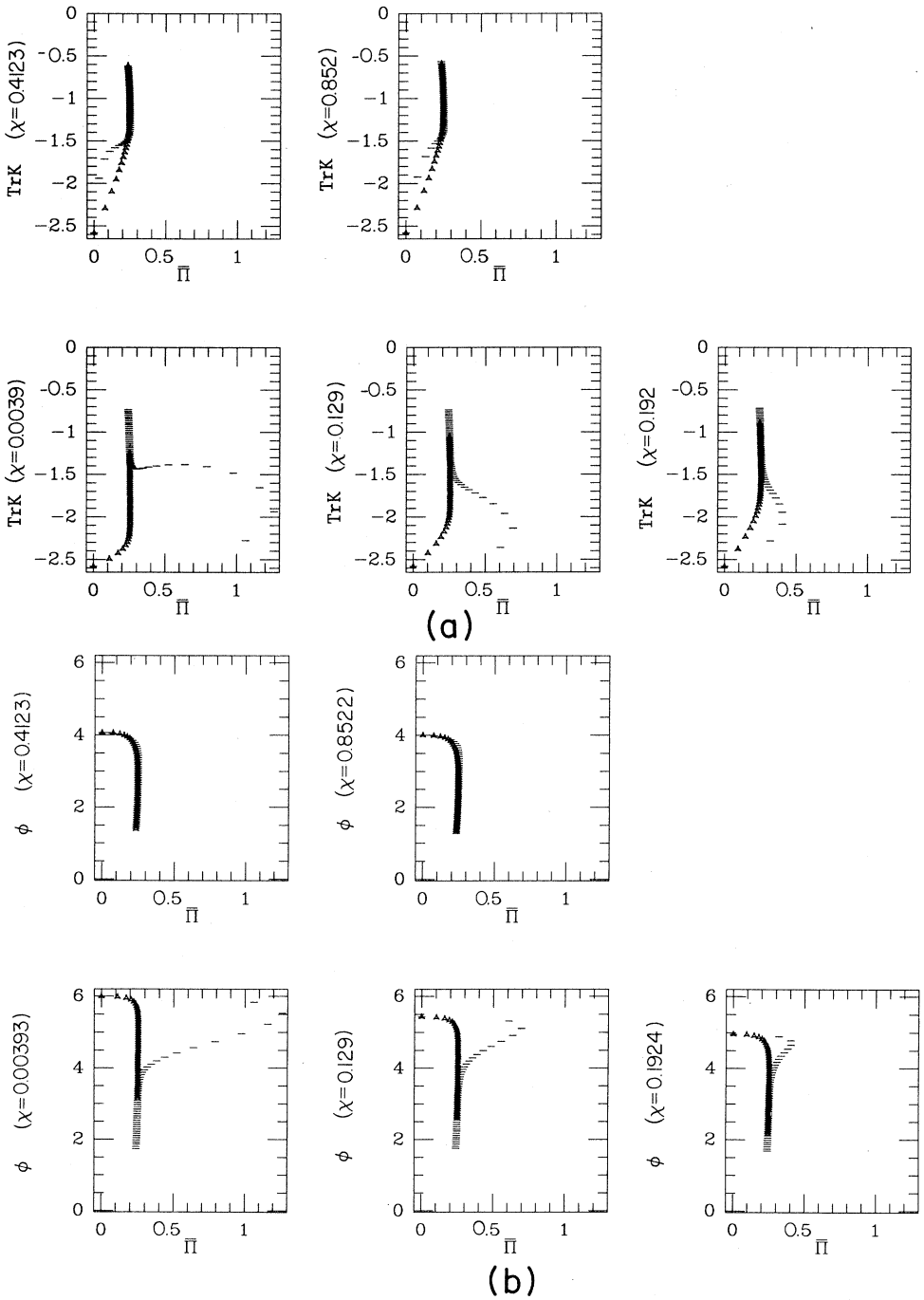

FIG. 10. (a) TrK vs $\bar{\Pi}$ trajectories of several points in a very inhomogeneous solution (bars) of Fig. 9 and the same curves in a homogeneous solution with the same initial data (triangles). The temporal evolution is in an increasing TrK direction. (b) Trajectories in the $\bar{\Pi}, \Phi$ plane for the same points. The temporal evolution is in a decreasing Φ direction.

geneous initial data. Again, this problem disappears with an appropriate choice of an additional radiation field (see Fig. 10).

Figures 6–11 describe the evolution of universes with both a massive scalar field and radiation. The initial overall density is homogeneous but the scalar field is of the form

$$\Phi_0=4+2\{\exp(-\chi^2/\Delta^2)+\exp[-(\pi-\chi)^2/\Delta^2]\}+\frac{4}{\Delta^2}(\chi-\pi/2)^2\exp(-\pi^2/\Delta^2)\ , \tag{5.3}$$

where $\Delta^2=0.8$ for Figs. 6–8 and $\Delta^2=0.05$ for Figs. 9–11. The initial momentum of the radiation field Π_Ψ is

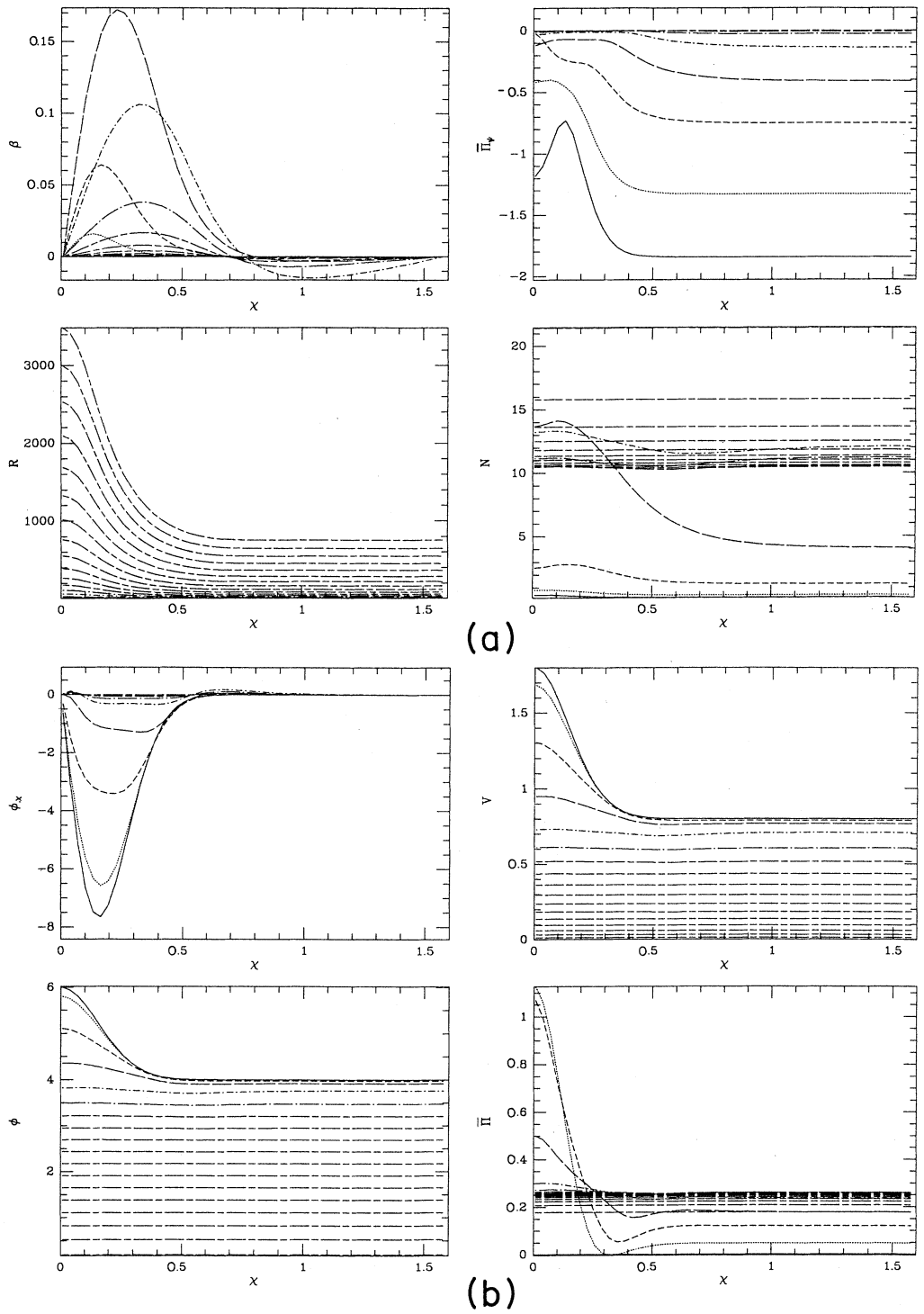

FIG. 11. Evolution of an inhomogeneous universe with the same initial data as in Fig. 9 but with $\mathrm{Tr}K=$const slicing condition (for details about the direction of the time see Fig. 2). (a) R, N, β, and $\overline{\Pi}_\Psi$ vs χ. (b) Φ, $\Phi_{,\chi}$, $\overline{\Pi}$, vs χ on different time slices.

given by

$$\Pi_\Psi = R^3\sqrt{2[\rho_0 - \rho(\Phi_0)]}\ , \tag{5.4}$$

so that the total energy density is constant and the initial data have an isocurvature form. The solution has an early phase during which the radiation field decays rapidly. After this period the scalar field dominates the evolution of the Universe.

In Figs. 6–8 the width of the scalar Gaussian was large (with $R_0=6$, $\rho_0=2.3$, and $\mathrm{Tr}K_0=-2.58$, $\Delta^2=0.8$ corresponds to $\approx 5.4H^{-1}$, i.e., to several horizon sizes). The inhomogeneity was, therefore, on a relatively large scale and it did not disturb the Universe from entering an inflationary phase. This can be seen clearly in Fig. 7 where we compare the evolution of the several points in an inhomogeneous universe with the evolution of homo-

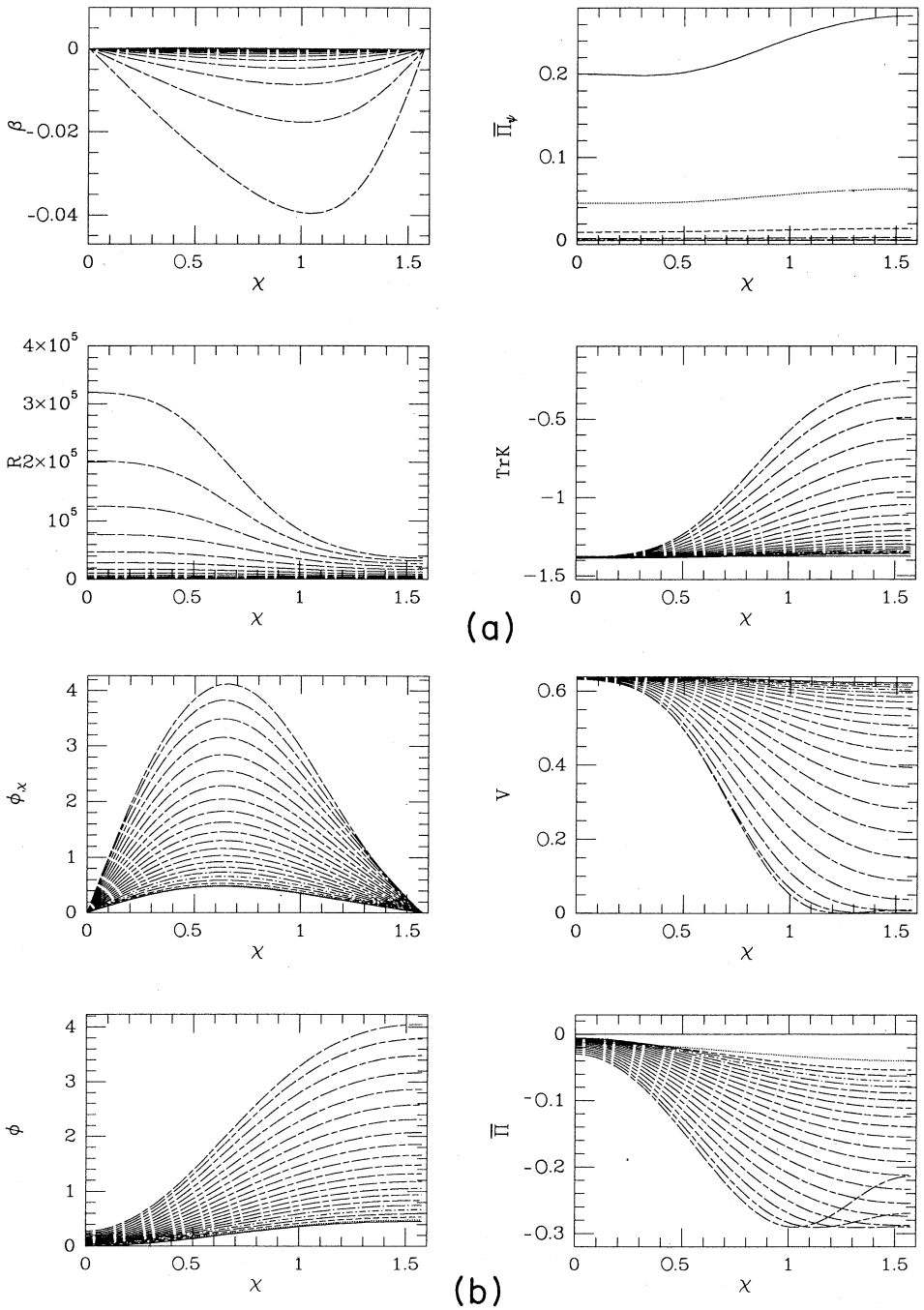

FIG. 12. Evolution of a universe with an isocurvature initial data combined of a "new-inflation"-type scalar field with $\Delta^2=0.8$ and a radiation field. $N=1$ slicing condition (for details about the direction of the time see Fig. 2). (a) R, $\mathrm{Tr}K$, β, and $\bar{\Pi}_\Psi$ vs χ. (b) Φ, $\Phi_{,\chi}$, $\bar{\Pi}$, and V vs χ on different time slices.

geneous universes with similar initial conditions (i.e., same values of R_0, $\mathrm{Tr}K_0$, Φ_0, and Π_0). It is evident that, apart from a small "rearrangement" period at the beginning of the solution, each point in the inhomogeneous universe behaves as if it is in a homogeneous universe with similar initial conditions.

Figure 8 displays the evolution of the same universe with $\mathrm{Tr}K=$const slicing conditions. The radiation field is sufficient, in this case, for this slicing condition to work. During the early phase of the evolution N is large in the inflationary region and it is small in the regions that do not inflate. This behavior of the lapse function is a typical indication for a situation in which one region of the Universe expands rapidly relative to the others. The lapse function N acts to slow the evolution in the region around $\chi=\pi/2$ in such a way that the source becomes homogeneous and the inhomogeneity of the slices is expressed only by variations in the value of R. The overall

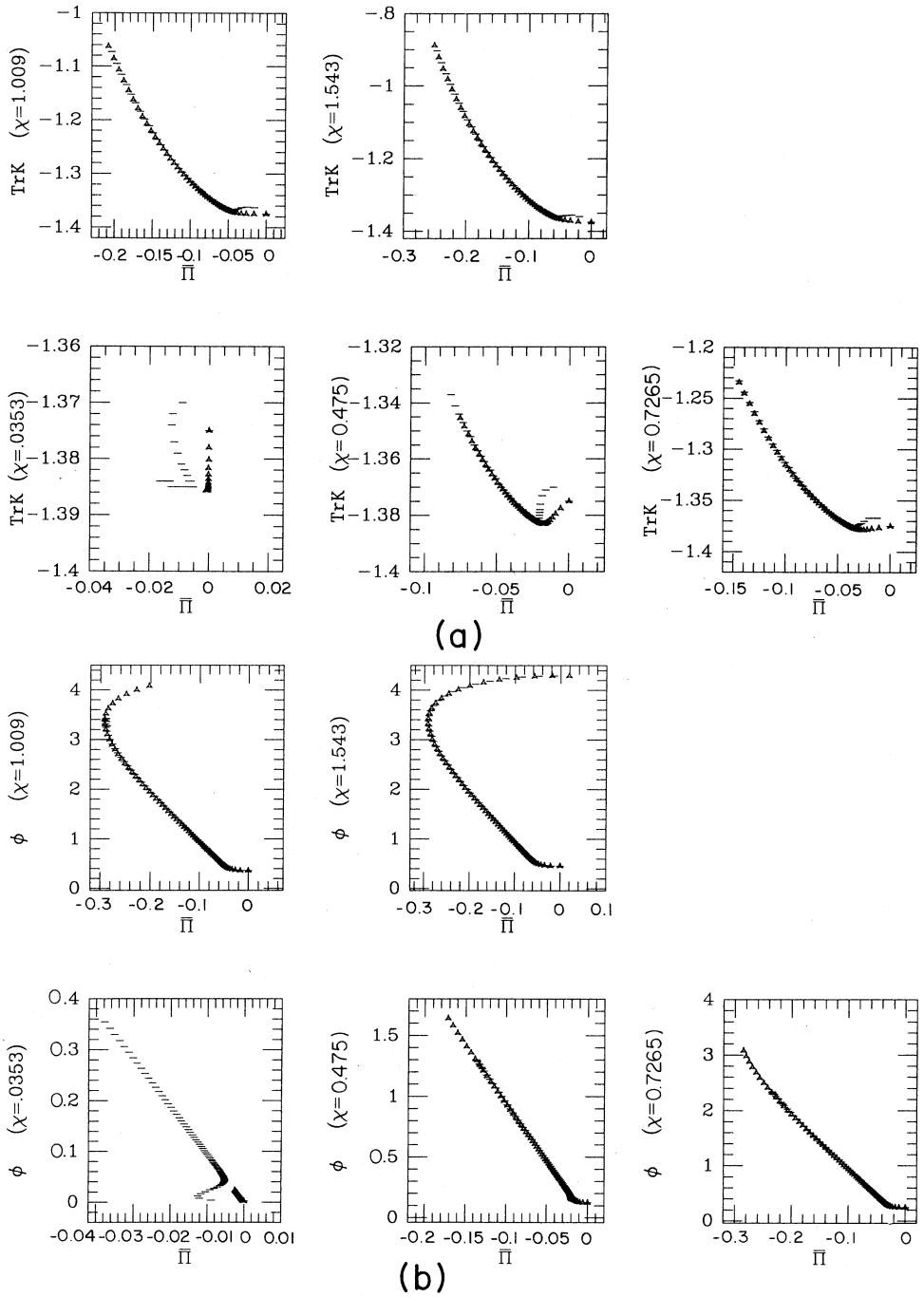

FIG. 13. (a) $\mathrm{Tr}K$ vs $\overline{\Pi}$ trajectories of several points in a "new inflation" inhomogeneous solution of Fig. 12 (bars) and the same curves in a homogeneous solution with the same initial data (triangles). The temporal evolution is in a decreasing Π direction. (b) Trajectories in the $\overline{\Pi},\Phi$ plane for the same points, the temporal evolution is in a decreasing Π direction.

similarity between this evolution and the one displayed in Fig. 6 suggests that the $N=1$ slicing condition is not so bad after all.

This situation has changed drastically when the width of the scalar-field distribution was decreased to $\Delta^2=0.05$ which corresponds to $\approx 1.2H^{-1}$. The evolution, as shown in Fig. 9, is different from the one shown in Fig. 6. There is almost no inflationary phase at all. The deviations from the homogeneous solutions are even clearer in Fig. 10, where we see that the phase $\overline{\Pi}\approx$const is much shorter then in the homogeneous solutions. When we evolve the same data with $\mathrm{Tr}K=$const slicing (Fig. 11) N does not have the same peak at the origin that it had when inflation occurred (see Fig. 8). This is probably the best indication that inflation does not take place with this initial data.

In Figs. 12 and 13 we display a universe containing a scalar field with a "new inflation" potential. The initial

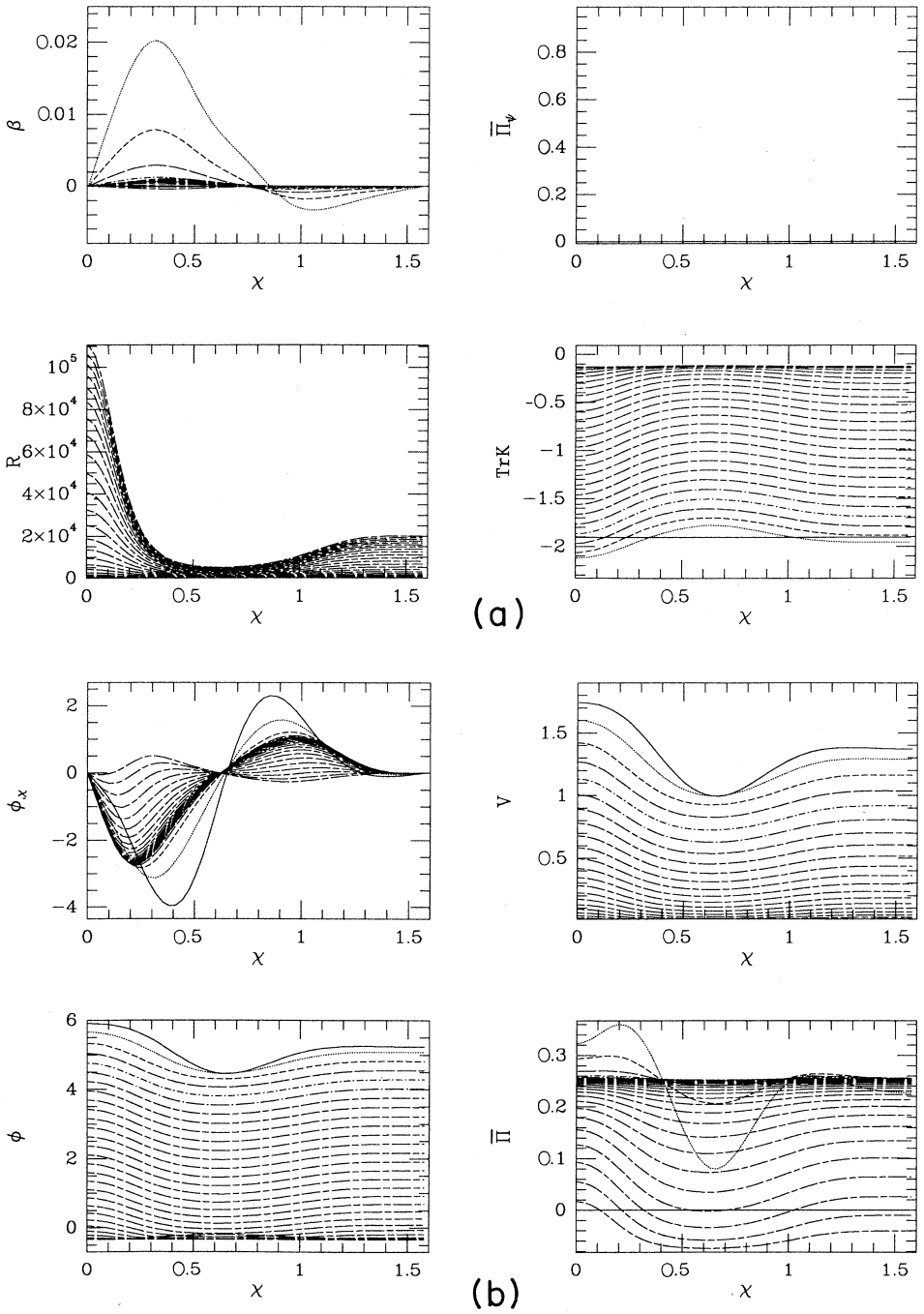

FIG. 14. Evolution of a universe with a massive scalar field, without a radiation field with $N=1$ slicing condition (for details about the direction of the time see Fig. 2). (a) R, $\mathrm{Tr}K$, β, and $\overline{\Pi}_\Psi$ vs χ. (b) Φ, $\Phi_{,\chi}$, $\overline{\Pi}$, and V vs χ on different time slices.

scalar field has the form

$$\Phi_0 = A\left[1-\exp(-\chi^2/\Delta^2)-\exp[-(\pi-\chi)^2/\Delta^2]\right.$$
$$-\frac{2}{\Delta^2}[(\chi-\pi/2)^2\exp(-\pi^2/\Delta^2)$$
$$\left.+(\pi/2)^2\exp(-\pi^2/\Delta^2)]\right]. \quad (5.5)$$

We used $A=0.5$ and $\Delta^2=0.8$. Again the perturbation is an isocurvature one and the scalar radiation field is given by Eq. (5.4), with this Φ_0. With this scalar-field configuration the central region inflates, while the outer region does not. The inflation at the center in the inhomogeneous case is much shorter than the inflation in the homogeneous case. This can be seen clearly by the great difference between the trajectories of the two solutions shown in Fig. 13. At the end of these calculations the scalar field at the outer regions oscillates around the minimum of its potential well.

Finally we display in Fig. 14 a universe with a massive scalar field but without a radiation field. Here we solve the initial-value problem using the modified York procedure and we cannot specify Φ arbitrarily. Our initial guess for Φ has a form similar to Eq. (5.3), but with 3 instead of 4 on the LHS and $\Delta^2=0.8$ [it looks like the solid curve for Φ in Fig. 6(b)]. This form changes during the modified York procedure as can clearly be seen by comparing the initial Φ (the solid curve for Φ) in Fig. 14 with the corresponding curve in Fig. 6(b).

VI. CONCLUSIONS

We have presented a numerical code for study of spherically symmetric cosmologies coupled to a scalar field. The code passed successfully several numerical tests. Preliminary results indicate that inhomogeneity does prevent inflation, and that a region of the size of the local horizon must be homogeneous in order that inflation will begin.

ACKNOWLEDGMENTS

It is a pleasure to acknowledge helpful discussions with R. H. Brandenberger, J. Katz, W. H. Press, W. Unruh, J. R. Wilson, and J. W. York. We thank the Institute for Theoretical Physics at Santa Barbara and the Department of Astronomy at Princeton University for their hospitality. The research was supported by a US-Israel Binational Science Foundation grant to the Hebrew University.

---

*Electronic address: Dalia@hujivms.BITNET.
†Electronic address: Tsvi@hujivms.BITNET

[1]A. H. Guth, Phys. Rev. D **23**, 347 (1981); see A. D. Linde, Rep. Prog. Phys. **47**, 925 (1984), for a review.
[2]See, for a review, M. S. Turner, in *General Relativity and Gravitation,* edited by M. A. H. MacCallum (Cambridge University Press, Cambridge, England, 1987).
[3]H. Kurki-Suonio, J. Centrella, R. A. Matzner, and J. R. Wilson, Phys. Rev. D **35**, 435 (1987), have calculated numerically the evolution of planar cosmological models with inflation.
[4]S. W. Hawking, Pont. Acad. Sci. Varia. **48**, 563 (1982); J. B. Hartle and S. W. Hawking, Phys. Rev. D **38**, 2960 (1983), S. W. Hawking, in *Relativity, Groups and Topology II,* proceedings of Les Houches Summer School, Les Houches, France, 1983, edited by R. Stora and B. DeWitt (Les Houches Summer School, Vol. 40) (North-Holland, Amsterdam, 1984).
[5]S. L. Shapiro and S. A. Teukolsky, Astrophys. J. Lett. **234**, L177 (1979).
[6]J. W. York, Phys. Rev. Lett. **28**, 1082 (1972); L. L. Smarr and J. W. York, Phys. Rev. D **17**, 2529 (1978).
[7]See, e.g., C. W. Misner, K. S. Thorne, and J. A. Wheeler, *Gravitation* (Freeman, San Francisco, 1973).
[8]T. Piran, in *The Early Universe,* edited by W. Unruh (Reidel, Dordrecht, 1988).
[9]J. R. Wilson, in *Sources of Gravitational Radiation,* edited by L. L. Smarr (Cambridge University Press, Cambridge, England, 1979).
[10]A. J. Goddard, Commun. Math. Phys. **54**, 279 (1977); D. Brill and F. Flaherty, *ibid.* **50**, 157 (1976).
[11]S. W. Hawking and G. F. R. Ellis, *The Large Structure of Space-Time* (Cambridge University Press, Cambridge, England, 1973).
[12]V. A. Belinski, L. P. Grishchuk, I. M. Khalatnikov, and Ya. B. Zel'dovich, Phys. Lett. **155B**, 232 (1985); T. Piran and R. M. Williams, *ibid.* **163B**, 331 (1985); T. Piran, Phys. Lett. B **181**, 235 (1986).
[13]J. A. Stein-Schabes, Phys. Rev. D **35**, 2345 (1987).
[14]See, e.g., R. M. Wald, *General Relativity* (University of Chicago Press, Chicago, 1984).